

Investigation of High-Temperature Slag/Copper/Spinel Interactions



EVELIEN DE WILDE, INGE BELLEMANS, MIEKE CAMPFORTS, MUXING GUO, BART BLANPAIN, NELE MOELANS, and KIM VERBEKEN

An important cause for the mechanical entrainment of copper droplets in slags during primary and secondary copper production is their interaction with solid spinel particles, hindering the sedimentation of the copper droplets. In the present study, the interactions between the three phases involved (slag–Cu droplets–spinel solids) were investigated using an adapted sessile drop experiment, combined with detailed microstructural investigation of the interaction zone. An industrially relevant synthetic $\text{PbO-CaO-SiO}_2\text{-Cu}_2\text{O-Al}_2\text{O}_3\text{-FeO-ZnO}$ slag system, a MgAl_2O_4 spinel particle, and pure copper were examined with electron microscopy after their brief interaction at 1523 K (1250 °C). Based on the experimental results, a mechanism depending on the interlinked dissolved Cu and oxygen contents within the slag is proposed to describe the origin of the phenomenon of sticking Cu alloy droplets. In addition, the oxygen potential gradient across the phases (*i.e.*, liquid Cu, slag, and spinel) appears to affect the Cu entrainment, as deduced from a microstructural analysis.

DOI: 10.1007/s11663-016-0805-8

© The Minerals, Metals & Materials Society and ASM International 2016

I. INTRODUCTION

IN primary and secondary copper smelting, the overall metal recovery is limited by copper losses in slags.^[1] When pursuing an improvement of the process efficiency by limiting the metal losses, it is an absolute prerequisite to obtain a fundamental understanding of the characteristics and origin of these metal losses.

It is well accepted, now, that copper losses in slags can be of chemical or mechanical nature.^[2–4] Chemical copper losses refer to the dissolution of copper as sulfide or oxide during primary copper production and mainly as oxide during secondary production. This type of losses is determined by the system thermodynamics and is intrinsic to pyrometallurgical processes. The main influencing factors are temperature, oxygen partial pressure,^[2,5–7] chemical activity of the metal,^[2] and composition of the slag and matte.^[2,5–7]

Mechanically entrained metal refers to entrapped or floating unsettled droplets. In primary copper production, both metallic and matte droplets are entrained,

while in secondary copper production, these losses are mainly metallic copper droplets. A variety of reasons are named in the literature to be responsible for this mechanical entrainment of droplets. Minto and Davenport^[8] suggested a source for entrained Cu: SO_2 bubbles, which originate at the bottom of the furnace, can elevate a surface film of matte into the slag.^[8–10] A second important source is the dispersion of precipitated copper or matte, due to a decrease of the copper solubility in the slag. This variation in solubility is related to the process inhomogeneity due to, for example, zones with a locally lower temperature or a locally different oxygen partial pressure.^[9] A third important cause is the entrapment of metal by manipulations such as charging or tapping. During tapping, mechanical entrainment can happen due to the rise of the underlying denser liquid phase, which can occur while flowing around obstacles in the vessel.^[3] The physical dispersion of the denser layer into the slag by mixing can have several causes such as turbulence, mixing one phase into the other or injecting gas.^[3,11] Additionally, the penetration of metallic copper into refractory can lead to metal losses.^[12] There exists, however, an important additional source of mechanically entrained droplets which have been omitted in most studies: the attachment of droplets to solids in slags, hampering the sedimentation. This observation was reported by Ip and Toguri^[9] and Andrews,^[11] and demonstrated for a synthetic slag system by De Wilde *et al.*^[13] These solids are often found to have a spinel structure. Even though the copper attachment to solid spinels was clearly observed,^[13] limited experimental or industrial data and fundamental insights concerning the active mechanisms are available.

A wide variety of methodologies has been applied to study metal losses in slags. A first frequently used approach uses water-based systems, representing the

EVELIEN DE WILDE, formerly Ph.D. Student with the Department of Materials Science and Engineering, Ghent University, Technologiepark 903, 9052 Zwijnaarde, Ghent, Belgium, is now Project Leader with Umicore R&D, Kasteelstraat 7, 2250 Olen, Belgium. INGE BELLEMANS, Ph.D. Student, and KIM VERBEKEN, Professor, are with the Department of Materials Science and Engineering, Ghent University. Contact e-mail: Inge.Bellemans@UGent.be MIEKE CAMPFORTS, Process Manager, is with Umicore R&D. MUXING GUO, Senior Researcher, BART BLANPAIN, and NELE MOELANS, Professors, are with the Department of Materials Engineering, KU Leuven, Kasteelpark Arenberg 44, bus 2450, 3001 Heverlee, Leuven, Belgium.

Manuscript submitted October 21, 2015.

Article published online September 7, 2016.

phases in the industrial process. The dispersion behavior of one liquid into another was studied by using oil/mercury,^[14] oil/water,^[15,16] and kerosene–water systems.^[3,15] A second approach is the use of models such as computational fluid dynamics,^[17] phase field models,^[18] or other numerical models simulating the process.^[19] A third frequently used methodology is the study of metal losses in slag by industrial and/or lab scale sampling procedures using industrial and/or synthetic slags.^[6,20–23] However, studies on the phenomenon of liquid metal droplets sticking to solid particles in slags have been limited. Recently,^[24] we investigated the phenomenon of sticking droplets in a synthetic PbO-based slag. Two possible sources were proposed to explain the origin of the sticking Cu droplets. Firstly, extensive stirring can be sufficient to induce the attachment. Secondly, it was suggested that sticking droplets can find their origin in a chemical reaction, happening when the system equilibrates.^[24]

Several experimental studies on the interaction between Cu alloys and slags with spinel particles are available. For the specific wettability of metals on spinel substrates, Kozlova *et al.*^[25] and Fukami *et al.*^[26] performed experimental studies on the wettability of iron on MgAl₂O₄ spinel substrates. As described in our previous work,^[13] the wetting behavior between Cu and Cu–Ag alloys on MgAl₂O₄ was examined in an oxygen partial pressure range between 10^{−13} and 10^{−8} atm using a sessile drop technique. A non-wetting behavior was observed for all alloys, with a maximal contact angle between 140 and 150 deg for the Cu–12.5 wt pct Ag alloy. With respect to oxygen partial pressure, pure copper showed an improved wetting for an oxygen partial pressure of 10^{−8} atm. For the Cu–Ag alloys, a less explicit effect of the oxygen partial pressure was observed, indicating a combined effect of oxygen partial pressure and the alloy composition.^[13] This could also explain the difference in observed trend as compared to the results of Pebo *et al.*^[27,28] They observed a lower surface tension (*i.e.*, a smaller contact angle) when the Cu–Ag alloys contained more Ag. One should note, however, that they used oxygen potentials consistently smaller than 10^{−15} atm, which could thus explain the difference in observed trend.

The comparison of the wetting behavior of copper on ZnFe₂O₄ and MgAl₂O₄ was performed using sessile drop experiments under a protective Ar atmosphere. A low wettability of copper was found for both spinels, but the contact angle for ZnFe₂O₄ (88 deg) was lower than on MgAl₂O₄ (123 deg).^[29] Even though, the spinel substrates had a different porosity and roughness, it gave an indication of the importance of the spinel composition on the wetting behavior.^[29]

The wettability between slags and spinels was also studied in the frame of slags attacking refractories and when studying the inclusion removal in steel refining. Abdeyzdan *et al.*^[30] examined the wettability of CaO–Al₂O₃–SiO₂–MgO slag on MgAl₂O₄ substrates. They found that the contact angle between the slag and the substrate displayed a fast decrease in the first seconds and reaches a plateau for extended times.^[30] Even for short time scales, slag reaction and penetration

were observed. Donald *et al.*^[31] studied the interactions between fayalite slags and synthetic spinels, representing refractory materials. Interfacial reaction products and dissolution of various refractory compounds into the slags were observed. In our previous work,^[32] we studied the interaction between MgAl₂O₄ and a synthetic PbO-based slag, revealing reactive wetting behavior and the fast formation of an interaction layer. However, no experiments focussing on the simultaneous copper–spinel–slag interaction have been reported, while this plays an essential role in practice as the three phases are present simultaneously in the real system.

The objective of the present study is to investigate the phenomenon of sticking copper droplets using an adapted type of sessile drop experiment, in which both slag and copper are molten simultaneously on a spinel substrate. This experiment was used to study the slag–copper–spinel interactions. Therefore, an industrially relevant synthetic slag system was used (PbO–CaO–SiO₂–Cu₂O–Al₂O₃–FeO–ZnO) to represent the slag. Magnesium aluminate (MgAl₂O₄) substrates and pure copper were chosen to represent the spinel phase and copper droplets, respectively. An extensive microstructural study was performed to study the spinel–copper–slag interactions with respect to the sticking behavior of copper droplets on the spinel particles.

II. EXPERIMENTAL PROCEDURE

A. Production of the Slag System

Slags were produced by melting oxides of appropriate quantities, corresponding to a slag composition in the spinel primary phase field, based on the thermodynamic calculations using FactSage6.4 thermochemical package (FACT and FT Oxid databases). The targeted slag composition is shown in Table I. FeO was added as a combination of metallic iron and hematite and CaO was added as limestone. 400 g of the targeted composition was weighed, mixed, and transferred in an Al₂O₃ crucible (270 mL). The Al₂O₃ crucible, surrounded by a protective SiC crucible, was heated in an inductive furnace (Indutherm, MU3000) up to a temperature of 1073 K (800 °C), under a protective N₂ atmosphere. At 1073 K (800 °C), the N₂ atmosphere was replaced by a CO/air mixture with volume ratio of 1 to 2.44, corresponding to an oxygen partial pressure (p_{O_2}) of 10^{−7} atm, with a total flow rate of 60 L/h. This atmosphere was kept constant during the remainder of the experiment. The slag was heated to 1473 K (1200 °C) and this temperature was kept for 30 minutes to melt all components. Subsequently, N₂ (60 L/h) was bubbled through the slag in order to homogenize the slag. Afterward, the induction furnace was kept at 1473 K (1200 °C) for 150 minutes. The high-temperature state of slag was obtained using a cold sampling bar, which was directly quenched in water and subsequently dried in a dry chamber at 423 K (150 °C).

A representative sample of the quenched slag was embedded in epoxy resin, ground, and polished using 9 μm and 3 μm diamond pastes. The sample was analyzed

Table I. Selected Targeted Synthetic Slag Composition Based on Thermodynamic Calculations Using FactSage

	ZnO	PbO	SiO ₂	Al ₂ O ₃	Cu	CaO	FeO
Weight percent	6.5	39.3	13.8	7.3	3.9	9.8	19.4

using light optical microscopy (LOM, Keyence VHX-S90BE) and electron probe microanalysis, using the backscattered electron (BSE) microscopy mode (EPMA-BSE, JEOL JXA-8530F). For the latter, the sample was coated with a conductive carbon layer.

The composition of the different phases is analyzed using a fully quantitative electron probe microanalysis–wavelength-dispersive spectroscopy system (EPMA-WDS, JEOL JXA-8530F), applying an acceleration voltage of 15 kV and a probe current of 15 nA. In microprobe analysis, elements are identified but not cations; therefore, cation proportions and mineral formulae must be recalculated using stoichiometric rules. However, some of the cations have more than one oxidation state (*e.g.*, Fe and Cu). Therefore, a choice must be made before the measurement, as it is associated with the choice of the standard used for the WDS measurements. These standards were selected carefully to obtain reliable measurements of the compositions of the quenched samples. The oxygen content of the slag phase and spinel particles was not measured directly. Instead, the oxidation state of the element was selected *a priori*. Although both Fe²⁺ and Fe³⁺ can be present, only ‘FeO’ was selected for the sake of simplicity for both the slag and spinel phases. However, the Fe³⁺/Fe²⁺ ratio can be estimated from Reference 33: $\text{Log}(\text{Fe}^{3+}/\text{Fe}^{2+}) = 0.17 \log(p_{\text{O}_2}) + 0.018 \text{ wt pct CaO} + 5500/T - 2.52$. A CaO equivalent can be used by including the ZnO and PbO contents as basic oxides. This results in a Fe³⁺/Fe²⁺ ratio of 1.29. In a similar way, ‘Cu₂O’ was chosen *a priori*, as both CuO and Cu₂O could be present in the slag phase according to Takeda *et al.*^[34] for the considered p_{O_2} . The composition of the copper alloy droplets entrained in the slag was measured in their elemental state.

B. Spinel Preparation

Spinel (MgAl₂O₄) substrates were produced using a spark plasma sintering equipment (type HP D25/1, FCT system Rauenstein, Germany, equipped with a 250 kN uniaxial press), as described in our previous work.^[13,29,35] The MgAl₂O₄ powder (Sigma-Aldrich, spinel nano powder, <50 nm particle size) was sintered at a temperature of 1573 K (1300 °C) under a load of 60 MPa. Subsequently, the sintered spinel plates were annealed at 1273 K (1000 °C) for 3 hours and were finally polished to a mirror finish using 9, 3, and 1 μm diamond pastes. The spinel phase was confirmed by XRD analysis, while some additional small corundum peaks were present in the XRD spectrum as well (Siemens diffractometer D5000). The roughness parameter R_A of the MgAl₂O₄ substrates has an average value of 0.19 +/−0.08 μm (Talysurf profilometer).

C. Sessile Drop Experiments

1. Setup

The interaction between MgAl₂O₄ and copper and slag was studied using an infrared heating furnace, included in the confocal scanning laser microscopy setup (Lasertec 1LM21-SVF17SP, CSLM). The infrared heating furnace allows fast heating and cooling by a 1.5 kW halogen lamp placed in the lower focal point of a small gastight ellipsoidal chamber that reflects the light to the other focal point where the observed sample is positioned. For this purpose, the ellipsoidal chamber is coated with Au to reflect the light. A programmable PID controller controls the temperature, read from a type B (Pt-6 pct Rh/Pt-30 pct Rh) thermocouple, which is part of the sample holder. An extra window is placed at the side of the heating chamber, combined with a camera (Ganz ZC-F10C3), which is placed on the same height, allowing to monitor the wetting of the droplet on the substrate. An oxygen gas analyzer is installed in the gas outlet to monitor the p_{O_2} variations in the heating chamber (Cambridge Sensotec LTD, Rapidox 2100).

2. Performed experiment

The simultaneous interaction of copper and slag with an MgAl₂O₄ substrate was evaluated under a protective Ar atmosphere. The MgAl₂O₄ substrate was cleaned ultrasonically in acetone and the copper was etched using a 1:1 H₂O:HCl solution to remove the outer copper oxide layer. The MgAl₂O₄ substrate was placed on the sample holder and leveled carefully. Subsequently, both copper and slag were placed on the substrate. The heating chamber was closed and flushed three times with Ar. First, the temperature was raised until 573 K (300 °C), with a heating rate of 50 K/min. After 1 minute at 573 K (300 °C), the temperature was increased further up to 1173 K (900 °C), with a heating rate of 200 K/min. After 1 minute at 1173 K (900 °C), the chamber was further heated up to 1523 K (1250 °C), which was then maintained for 8 minutes. Finally, the sample was cooled down with a cooling rate of 500 K/min. The complete process, starting from the melting of the droplet till the final cooling, was monitored.

The average weights of slag and copper during the sessile drop experiments were 0.0175 and 0.022 g, respectively. The experiment was repeated multiple times to ensure the reproducibility of the observations. The monitored p_{O_2} value during the experiments varied between 6.5×10^{-3} and 7.5×10^{-5} atm.

The obtained sessile drop sample was embedded (Technovit 4000 powder and liquid), ground until the cross-section between the spinel substrate and copper/slag became visible and then polished using 9, 3, and 1 μm diamond pastes. Samples were analyzed using LOM and BSE (EPMA). The latter was also combined

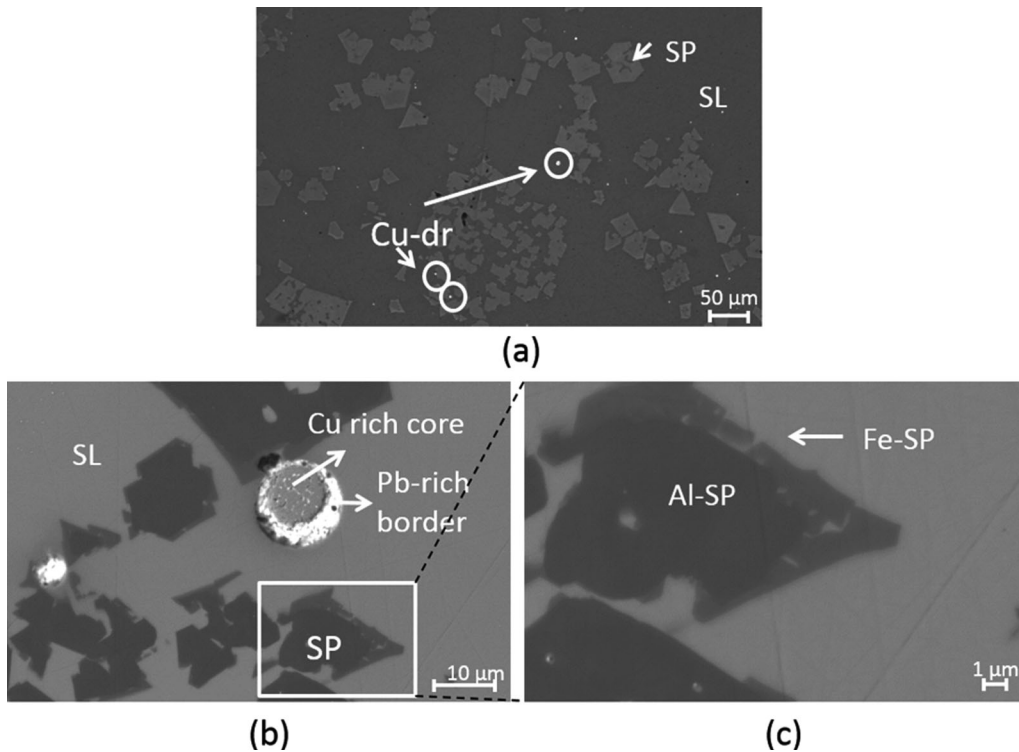


Fig. 1—Representative LOM (a) and BSE (b, c) images of quenched slag system obtained after 150 min equilibration at 1523 K (1250 °C). (SP, spinel; SL, slag; Cu-dr, Cu alloy droplets; Al-SP, Al-rich spinel phase; Fe-SP, Fe-rich spinel phase).^[32]

Table II. Overview WDS Analysis of the Slag, Fe-Rich Spinel Phase, and Al-Rich Spinel Phase.^[32]

Weight Percent	Al ₂ O ₃	'FeO'	'Cu ₂ O'	CaO	ZnO	PbO	SiO ₂
Slag	7.1	16.1	1.3	8.7	5.5	36.4	25.7
Al-rich spinel	36.9	39.7	0	0	22.5	0.1	0.2
Fe-rich spinel	17.7	63.6	0.1	0	14.3	0.3	0.4

Table III. WDS Analysis of Cu-Rich Core and the Pb-Rich Border of the Present Cu-Pb Alloy Droplets.^[32]

Weight Percent	O	Al	Fe	Cu	Ca	Zn	Pb
Cu core	0.7	0	1.5	95.0	0	0.5	1.2
Pb-rich border	3.4	0	1.4	1.9	0.12	0.9	92.3

with WDS analysis (EPMA, acceleration voltage = 15 kV; probe current = 15 nA) to determine the chemical compositions, as explained in Section II-A.

III. RESULTS

A. Microstructural Analysis of the Slag System

Representative LOM and BSE microstructure images of the slag phase after quenching are shown in Figure 1. Three phases are present as follows: slag (SL), spinel (SP), and copper droplets (Cu-dr) (indicated on Figure 1). Some of the present copper droplets display a sticking behavior to spinel particles, as shown in Figure 1(b). WDS analysis has been performed on the slag phase, spinel particles, and copper droplets. The resulting compositions are summarized in Table II. The composition of the slag itself changed compared to the targeted composition as shown in Table I. For Cu, this can be explained by the formation of alloy droplets within the slag phase. Pb will partition toward this alloy

phase, in accordance with the findings of Takeda *et al.*,^[34] resulting in a lower PbO content of the slag as shown in Table II. Takeda *et al.*^[34] also showed that Zn partitions toward the slag phase, but the amount of ZnO in Table II is lower than the start composition in Table I as it is one of the major spinel-forming components.

The spinel solids consist of the three spinel-forming components in the slag (*i.e.*, 'FeO,' ZnO, and Al₂O₃). Certain spinel solids consist of two phases, namely a Fe-rich spinel phase at the border (Fe-SP) and Al-rich spinel phase in the core (Al-SP) of the particle, (Figure 1(c)). Certain spinel particles consist completely of the Fe-rich spinel phase. In the remaining text, only the Fe-rich spinel is considered, as this Fe-rich spinel phase forms the outer layer of the spinel particles and is therefore in direct contact and local equilibrium with the slag system.

The WDS analysis of the copper alloy droplets is summarized in Table III. Under the present experimental conditions, Cu-Pb droplets with a phase separation between a Cu-rich core and a Pb-rich border are formed,

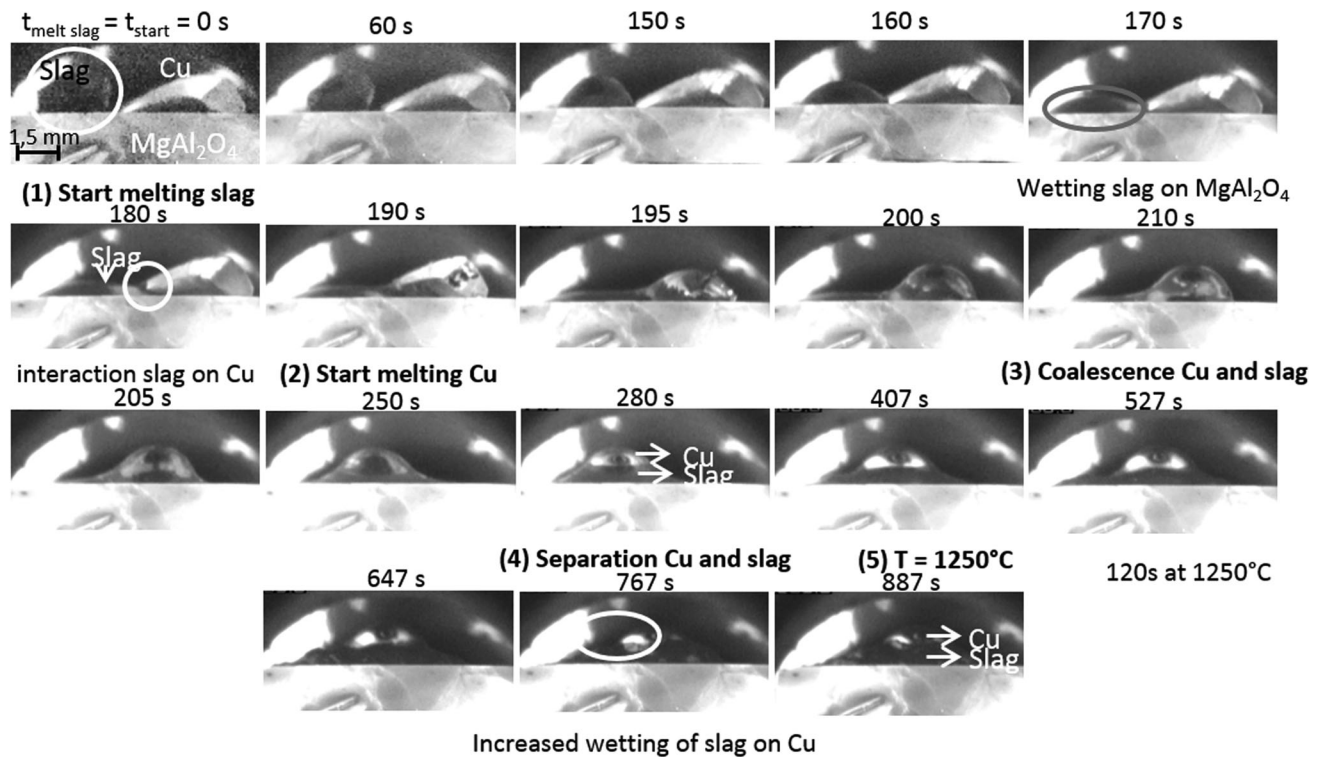


Fig. 2—Screenshots illustrating the melting and wetting behavior of copper and the produced synthetic slag on the MgAl_2O_4 substrate. The melting point of the slag is taken as the zero-point for the timescale ($t_{\text{melt slag}} = t_{\text{start}} = t_0$). Four different stages were defined within the melting and heating processes: (1) melting of the slag, (2) melting of the copper, (3) coalescence of Cu and slag, and (4) separation of copper and slag.

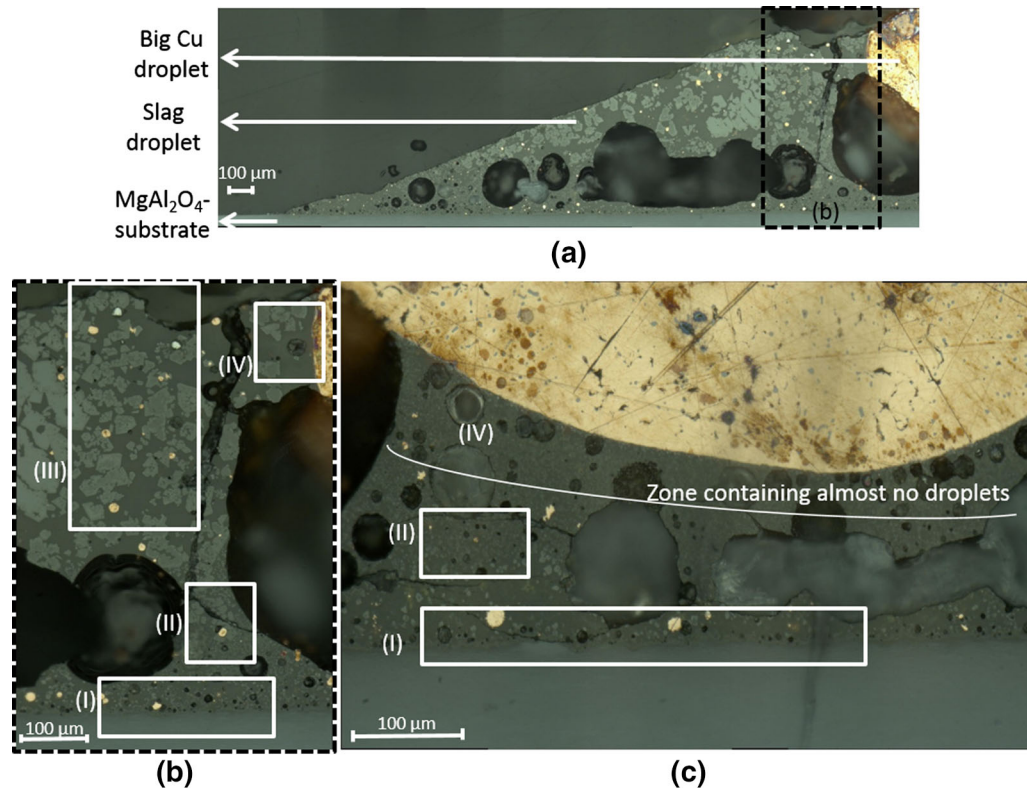


Fig. 3—LOM of the cross-section of the slag–copper– MgAl_2O_4 sessile drop sample. (a) General overview of slag droplet and copper droplet on the substrate. (b) Detailed overview of the microstructure of the slag droplet on the left side of the copper droplet, in which four zones can be distinguished: (I) MgAl_2O_4 –slag interface, (II) lower slag layer containing very small spinel solids, (III) upper slag layer containing entrained copper droplets, and (IV) slag–copper droplet interface. (c) Detailed overview of the slag underneath the copper droplet.

as shown in Figure 1. The phase separation is a direct consequence of the low Pb solubility in Cu at lower temperatures, and therefore, this phase separation is not present at high temperature during the experiment.

B. Spinel–Copper–Slag Interaction

1. Melting, wetting, and interaction behavior of copper and slag on $MgAl_2O_4$

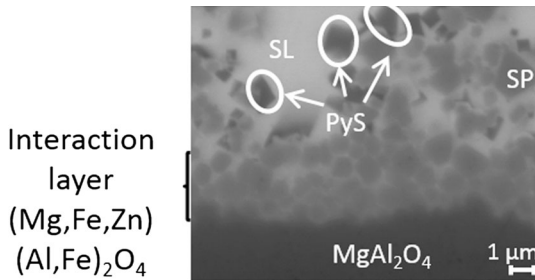


Fig. 4—Detailed BSE image of the formed interaction layer $(Mg,Fe,Zn)(Al,Fe)_2O_4$ at the slag– $MgAl_2O_4$ interface (zone I). The slag (SL) directly positioned above the interaction layer contains spinel particles (SP) and pyroxene solids (PyS).

A typical example of the melting and wetting behavior of slag and copper on a spinel substrate is presented in Figure 2 using the screenshots obtained during the monitoring of the experiment. The wetting behavior can also be observed in a supplementary video file. The moment at which the slag starts to melt is regarded as the start of the experiment and is chosen as zero-point for the timescale of the experiment ($t_{\text{melt slag}} = t_{\text{start}} = t_0 = 0$ s). Four different stages can be distinguished, as indicated in Figure 2. In a first stage, the slag droplet melts. Once the slag is molten, a very good wetting behavior of the slag on the spinel substrate is observed (Figure 2—170 seconds). Additionally, the slag seems to wet the copper droplet, which is still solid at this point, as indicated on the captured image after 180 seconds. (Figure 2) In a second stage, the copper droplet melts, displaying a limited wetting behavior on the spinel substrate as compared to the slag system. Once the copper droplet is melted, the liquid copper and slag start to interact (195 to 205 seconds) and after 250 seconds, both liquid phases coagulate into one droplet, which is defined as stage (3). Subsequently, within a very limited time frame, a phase separation between the two liquid phases takes place (stage (4)), during which the slag sinks and spreads on the spinel substrate. The liquid copper stays on top of the slag, as

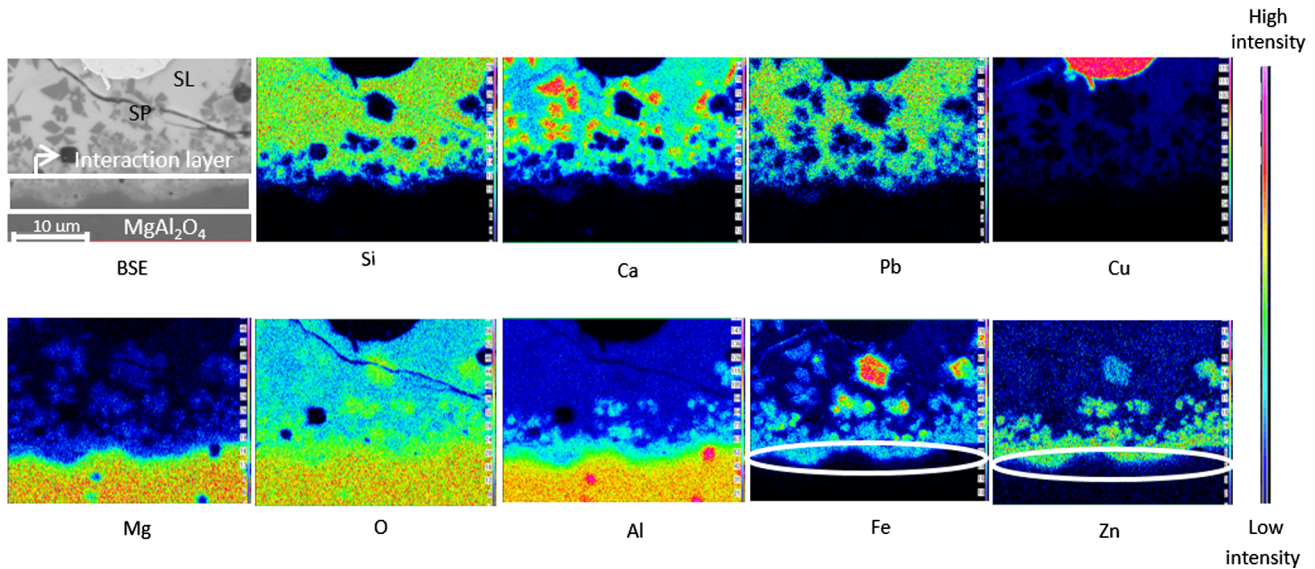


Fig. 5—WDS elemental mappings of the slag– $MgAl_2O_4$ interface in zone I. On the elemental mappings of Zn and Fe, the diffusion zone of both elements in the upper layer of the $MgAl_2O_4$ substrate is indicated. (SL, slag; SP, spinel).

Table IV. WDS Analysis of the Interaction Layer ($MgAl_2O_4$ Substrate Side and Slag Phase Side of the Layer), the Slag, Spinel Solids, and Pyroxene Solids in Zone I

Weight Percent	Al_2O_3	MgO	'FeO'	' Cu_2O '	CaO	ZnO	PbO	SiO_2
$MgAl_2O_4$ side of the interaction layer	66.5	20.2	3.9	1.1	0.1	5.5	0	0.1
Slag side of the interaction layer	44.3	8.1	23.3	1.6	0.8	18.0	1.5	3.1
Slag	13.1	0.8	5.7	5.7	10.6	1.6	23.6	37.8
Spinel solids	19.5	5.1	60.8	2.7	0.4	9.1	0.5	1.2
Pyroxene solids	14.3	4.8	15.6	1.6	20.8	0.9	4.9	37.4

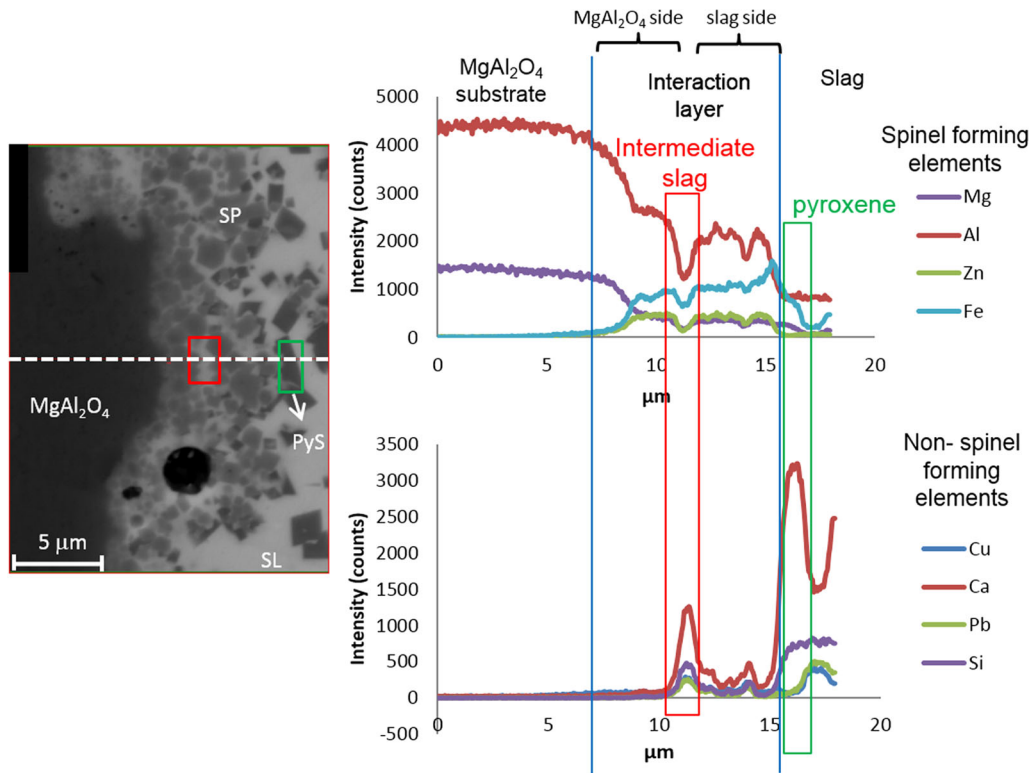


Fig. 6—Elemental WDS line scans of the slag– MgAl_2O_4 interface, indicated on the left BSE microstructure. The upper graphs represent the compositional evolution at the interface for the spinel-forming elements. The lower graphs show the evolution of the interface of the main slag-forming elements.

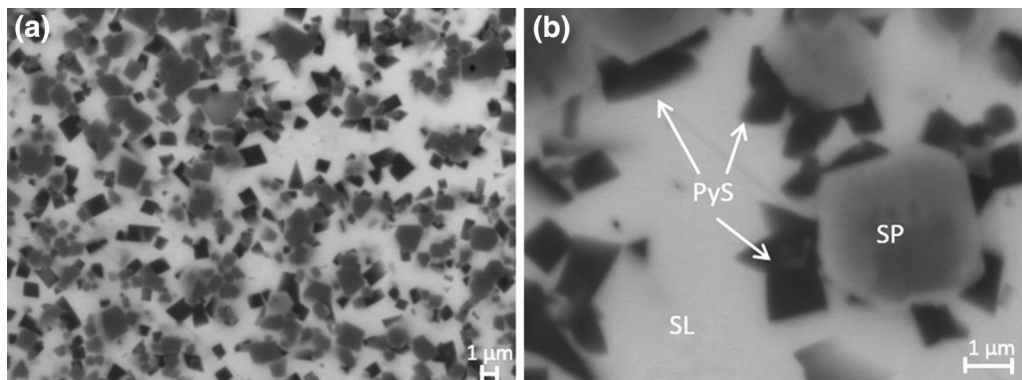


Fig. 7—Representative BSE images from the slag above the slag– MgAl_2O_4 interface (zone II) (a) general overview, (b) detailed microstructure (SL, slag; SP, spinel; PyS, pyroxene solids).

indicated in Figure 2—280 seconds. This image gives the impression that the copper droplet is not in contact with the MgAl_2O_4 substrate. Based on the densities of copper and slag, the opposite behavior would be expected.

The MgAl_2O_4 –copper–slag system was kept for 8 minutes at 1523 K (1250 °C). During this interaction time at 1523 K (1250 °C), it is observed that the slag tends to wet the copper droplet as a gradual increase in the contact area between slag and copper droplet is observed on the screenshots (Figure 2).

2. Microstructural analysis

In Figure 3, LOM images of the cross-section of the slag–copper– MgAl_2O_4 sample are shown. Figure 3(a) represents a general overview of the slag and copper droplet on the MgAl_2O_4 substrate. This microstructural analysis confirms the assumption that there is no direct contact between the MgAl_2O_4 substrate and the copper droplet. A more detailed image of the slag phase directly next to the copper droplet, indicated by the box in Figure 3(a), is given in Figure 3(b). The slag phase next to the droplet on the MgAl_2O_4 substrate can be roughly

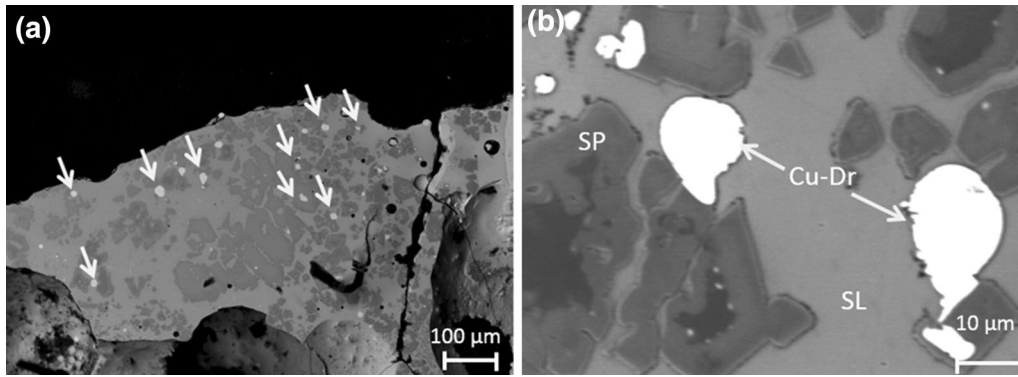


Fig. 8—Representative BSE images of the microstructure of the upper slag layer (zone III) (a) General overview, indicating the presence of small entrained copper droplets sticking to spinel particles (b) detailed image small entrained sticking copper droplets (SL, slag; SP, spinel; Cu-Dr, small entrained copper droplet).

Table V. WDS Analysis of the Spinel Solids and Slag in Zone III

Weight Percent	Al ₂ O ₃	MgO	'FeO'	'Cu ₂ O'	CaO	ZnO	PbO	SiO ₂
Spinel (absence of sticking Cu-dr)	14.9 ± 2.5	1.5 ± 0.8	65.1 ± 2.4	1.5 ± 0.6	0.1 ± 0.04	15 ± 3.8	0.1 ± 0.04	0.2 ± 0.1
Spinel (next to sticking Cu-dr)	12.7 ± 1.4	1.9 ± 0.5	70.8 ± 1.7	2.5 ± 0.3	0.4 ± 0.2	10 ± 1.4	0.1 ± 0.03	0.2 ± 0.04
Slag (average)	11.7	0.9	8.4	5.9	11.2	1.9	23.2	35.9

For the spinel solids, a distinction was made between spinel solids, not sticking to small entrained copper droplets and spinel solids positioned directly next to a small entrained copper droplet.

Table VI. WDS Analysis of the Small Entrained Copper Droplets, Displaying a Sticking Behavior Toward Spinel Solids (Zone III)

Weight Percent	O	Al	Mg	Fe	Cu	Ca	Zn	Pb	Si
Cu	0.5	0	0	2.0	97.5	0.1	0.3	0.1	0.1

subdivided into four main parts based on their microstructural characteristics: (I) the slag–MgAl₂O₄ interface, with a visible interaction layer, (II) the lower slag layer containing finely dispersed spinel solids, (III) the upper slag layer with a similar microstructure as the unreacted slag, containing small entrained copper droplets, and (IV) the interface between the slag and the copper droplet. Figure 3(c) gives a detailed LOM image of the slag region positioned between the MgAl₂O₄ substrate and the copper droplet. Similarly to the previous image (Figure 3(b)), zones (I), (II) and (IV) can also be distinguished here. Zone (III) was probably only observed in micrograph (b) and not in (c), because it is situated furthest from both the slag–substrate and the slag–droplet interface and thus changes the least. Moreover, it becomes clear that the slag in zone (IV) does not contain any copper droplets, in contrast with the other slag zones. The microstructural characteristics of each zone (I, II, III, IV) are studied in more detail, and are discussed below.

A more detailed image of the interface between the MgAl₂O₄ substrate and the slag droplet (zone I) is shown in Figure 4. A WDS mapping of all present elements is shown in Figure 5 which is taken from a

similar place as Figure 4. Quantitative WDS analysis of the different phases was performed using EPMA and is listed in Table IV. A line scan of the same region is presented in Figure 6. The clear formation of an interaction layer at the slag–MgAl₂O₄ interface can be observed from both the line scan and the WDS analysis. For convenience, the lines that demarcate the interaction layer are defined to be between 90 and 20 pct of the amount of Al present in the MgAl₂O₄ substrate. This layer has a (Mg,Fe,Zn)(Al,Fe)₂O₄ structure. The composition of the interaction layer varies along the position in this layer, as can be seen on the elemental mappings and line scans of the spinel-forming components (Mg, Al, Fe, and Zn). Close to the substrate, the interaction layer consists of MgO and Al₂O₃, originating from the MgAl₂O₄ substrate. Closer to the slag, the spinel-forming elements present in the slag become more prominent (Table IV).

The slag bordering next to the interaction layer contains both spinel solids (SP) and dark particles, as indicated in Figure 4. Based on the WDS analysis (Table IV) and the line scan (Figure 6), the dark solids can be identified as pyroxene. Due to the very small dimensions of these solids, it is very difficult to quantify

the amounts of Fe and Al precisely and to determine the chemical formula. Based on the composition, it could be suggested that the solids are hedenbergite ($\text{CaFeSi}_2\text{O}_6$), with a part of the Si cations replaced by Al cations. In order to maintain electrical neutrality, an excess of Fe cations is present.

The slag, spinel, and pyroxene solids all contain MgO, originating from the MgAl_2O_4 substrates, which indicates its dissolution. Additionally, an increase of the amount of Al_2O_3 in the slag compared to the slag composition before the experiment (Table II) confirms that the MgAl_2O_4 dissolves into the slag. Based on the elemental mappings of Fe and Zn, it appears that ZnO and 'FeO,' referring to both FeO and Fe_2O_3 , diffused into the upper part of the spinel substrate (Figure 5). However, the gradients in composition seen on the

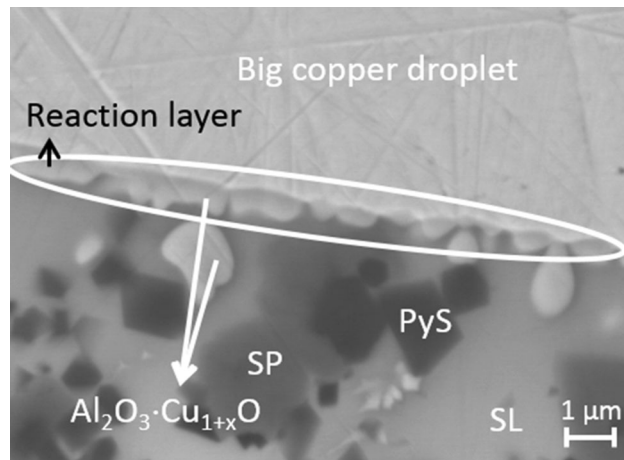


Fig. 9—Detailed BSE image of the slag–copper droplet interface (zone IV), on which a Cu-oxide layer is visible. (SL, slag; SP, spinel; PyS, Pyroxene solid).

elemental maps could also be due to an interference with the interaction layer. Thus, where, in the absence of a spinel phase, Zn clearly partitions toward the slag phase (Takeda *et al.*^[34]), it can be observed that this is no longer the case when spinel particles are present in the system as ZnO is clearly a spinel-forming element: the concentration of ZnO on the 'slag side of the interaction layer' is larger than in the slag itself, as represented in Table IV. No diffusion of the other slag-forming oxides (PbO , CaO , SiO_2 , and ' Cu_2O ') in the direction of the MgAl_2O_4 substrate is observed.

A representative BSE image of the lower slag layer (zone II) is shown in Figure 7(a). This part of the slag consists of very small spinel and pyroxene solids, as indicated in the detailed microstructure in Figure 7(b). Both the spinel and pyroxene solids have comparable compositions as the spinel and pyroxene solids positioned directly above the slag– MgAl_2O_4 interface (Table IV). This was confirmed by the WDS analysis which was performed on this sample, but which is not shown for reason of conciseness.

The upper slag layer (zone III) has a similar microstructure as the unreacted slag described in Section III–A. It contains bigger spinel solids and no pyroxene solids are present. However, it can be noted that smaller entrained copper droplets exist in the slag, which display a sticking behavior to the spinel solids, as indicated in Figure 8(a). For the sake of clarity, those sticking droplets will be referred to as 'small entrained sticking copper droplets' throughout this paper, while the large copper droplet, which is on top of the slag, will be referred to as 'copper droplet.' Figure 8(b) shows a detailed BSE image of the small entrained sticking copper droplets. A complete wetting between the present spinel solids and copper within the slag is noted, which will be elaborated in detail further on in this paper. EPMA-WDS analysis of the slag, spinel solids, and small entrained sticking copper droplets are summarized

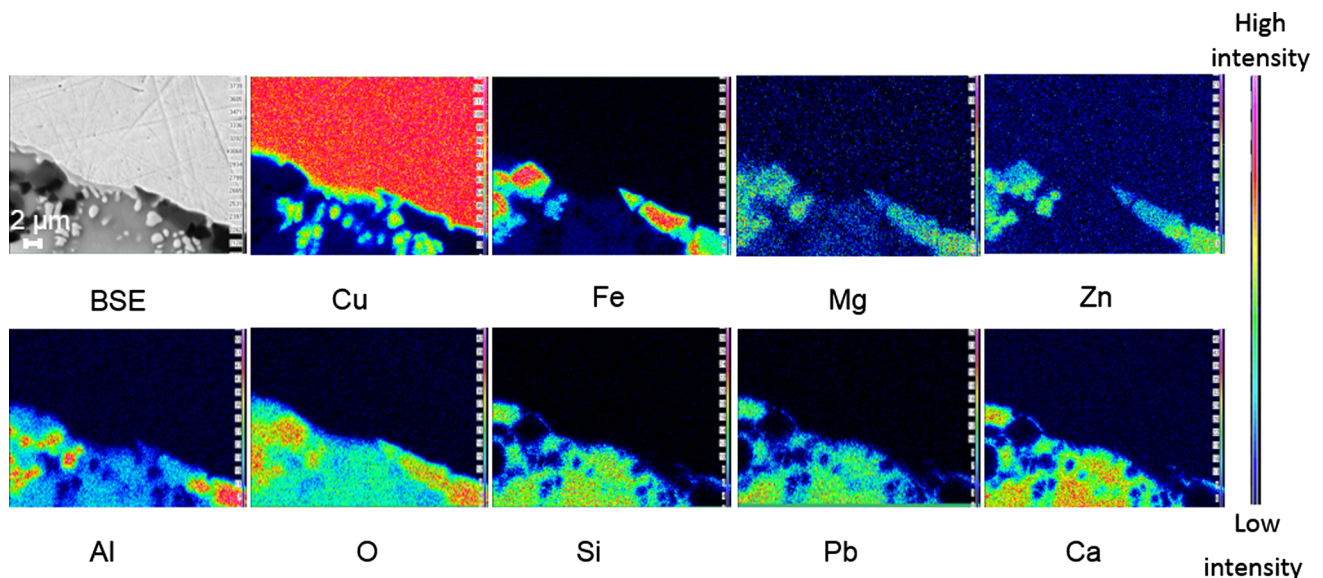


Fig. 10—WDS elemental mapping of the slag–copper droplet interface (zone IV).

Table VII. WDS Analysis of the Spinel Solids, Slag, Pyroxene Solids, and Cu-Oxide Layer Present in Zone IV

Wt Pct	Al ₂ O ₃	MgO	'FeO'	'Cu ₂ O'	CaO	ZnO	PbO	SiO ₂
Slag	10.3	0.6	4.5	8.0	8.8	1.1	34.6	32.5
Spinel	15.1	4.0	61.1	5.51	0.7	9.9	1.4	1.4
Cu-oxide layer	0.6	0.1	0.8	98.6	0.43	0.3	1.4	2.2
Pyroxene	13.3	3.1	15.9	3.5	15.9	1.5	16.9	29.7

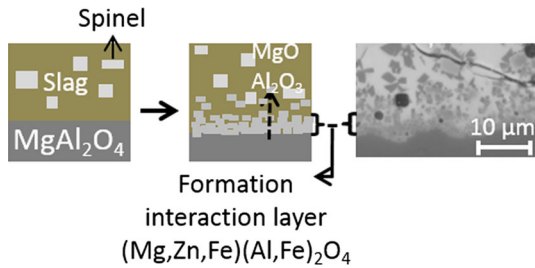


Fig. 11—Schematic representation of the slag–MgAl₂O₄ interface showing the formation of the interaction layer and the dissolution of MgO and Al₂O₃ into the slag.

in Tables V and VI. Additionally, EPMA-WDS analysis of the spinel solids positioned exactly next to small entrained sticking copper droplets are also given. The spinel solids in direct contact with small entrained sticking copper droplets contain higher amounts of 'FeO' and 'Cu₂O' compared to the spinel solids which are not in contact with small entrained copper droplets. Furthermore, it should also be noted that the amount of 'Cu₂O' dissolved in the slag depends on the position. The slag positioned further away from the copper droplet contains less copper, compared to the slag closer to the droplet. In Table IV, an average value for the slag is given throughout the entire zone.

Zone (IV) focusses specifically on the slag–copper droplet interface. A detailed BSE image of the microstructure is given in Figure 9. Similar for zone (I) and (II), the slag contains spinel and pyroxene solids. However, no metallic copper droplets are present in this zone, as already noted on the LOM images (Figure 3). At the interface of the big copper droplet and the slag, a clear interaction is visible, as indicated in Figure 9. A qualitative WDS mapping of the slag–copper interface is shown in Figure 10. Quantitative WDS data are summarized in Table VII. Both the slag phase and the spinel solids positioned next to the copper droplet (Table VII) contain more copper, 8.0 and 5.5 wt pct, respectively, compared to the slag in the other zones. On the elemental mappings of oxygen and copper, it can be seen that the reaction layer has a lower intensity compared to the metallic copper from the copper droplet and that oxygen is present. Moreover, some aluminum (coming from the slag phase) is also present at that position, indicating that the reaction layer consists of Cu_{1+x}O–Al₂O₃, of which the possible formation was confirmed by FactSage calculations. This assumption was confirmed by the qualitative WDS analysis, presented in Table VII.

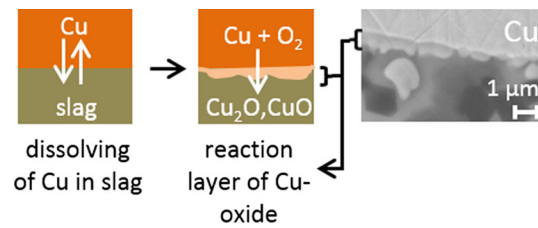


Fig. 12—Schematic representation of the slag–copper droplet interface showing the dissolution of copper into the slag, combined with the formation of the reaction layer of copper oxide.

IV. DISCUSSION

The adapted sessile drop experiment allows the simultaneous study of the interactions between both liquid slag and liquid copper with a solid spinel MgAl₂O₄ substrate. Consequently, the three relevant interactions that determine the phenomenon of sticking copper droplets in slags could be examined. In our experiment, the slag/spinel/copper interactions were studied using MgAl₂O₄ substrates, a synthetic PbO-based slag and pure copper to represent the spinel solids, the industrial slags, and the sticking copper droplets, respectively.

A. Study of Spinel–Slag, Spinel–Copper, and Copper–Slag Interactions Within the Sessile Drop Experiments

Based on the obtained screenshots, it was observed that when both slag and copper were molten, both liquids coalesce shortly. Subsequently, the slag phase spreads on the MgAl₂O₄ substrate and positions itself in between the liquid copper and the spinel substrate. However, based on the copper and slag density, the opposite behavior is expected. This can be explained by the very low masses of slag and copper used in the sessile drop experiment. Therefore, the gravity effect on the droplets is negligible and it is assumed that the interfacial tensions between the spinel substrate and both liquids will be the dominant factor in our experiment.^[36]

On the screenshots (Figure 2) and the microstructure of the cross-section (Figure 3), no copper–MgAl₂O₄ interface is observed due to the presence of the slag between both phases. This is in agreement with the outcomes of standard sessile drop experiments in the literature, where copper alloys are generally found to display a non-wetting behavior with respect to spinel substrates. In the literature, the spinel composition,^[29,36] alloying elements,^[13] and the oxygen partial pressure^[13,37] are all quoted to have an important influence

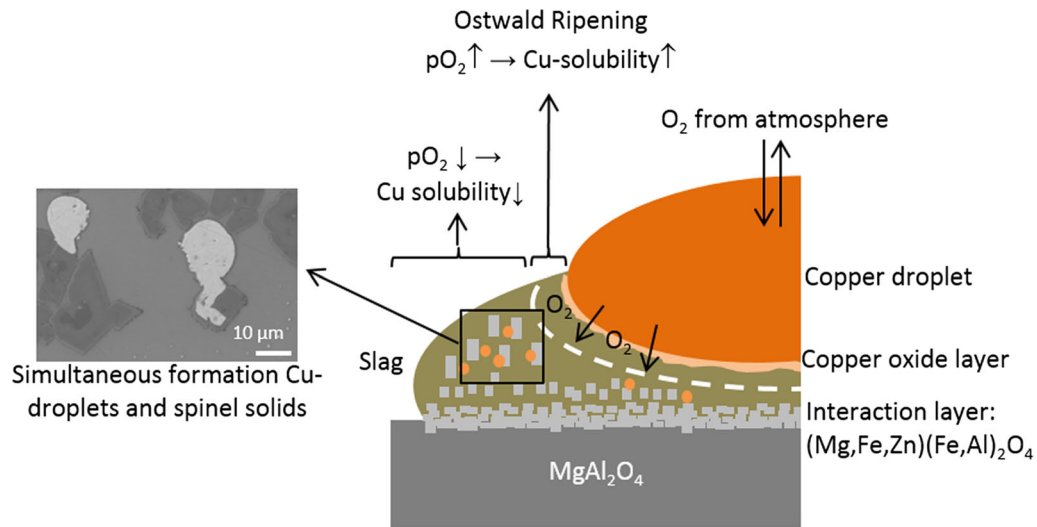
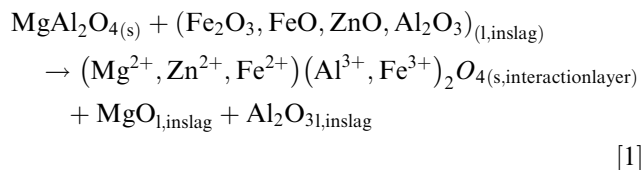


Fig. 13—Schematic representation of the proposed pathway to explain the presence of small entrained copper droplets in the slag droplet, displaying a sticking behavior to spinel particles in slags.

on the wetting behavior, but the lowest experimentally observed contact angle between magnetite and copper still was around 60 deg, with an estimated oxide dissolution (molar fraction) of 10^{-3} in the liquid metal.^[36]

In contrast to copper, the slag displays a very good wetting on the MgAl_2O_4 substrate, as shown on the screenshots in Figure 2. Microstructural investigation of the slag– MgAl_2O_4 interface showed the formation of an interaction layer, consisting of $(\text{Mg,Zn,Fe})(\text{Al,Fe})_2\text{O}_4$, with a chemical composition dependent on the distance from the MgAl_2O_4 substrate. The formation of the interaction layer demonstrates that the slag displays a reactive wetting behavior on the MgAl_2O_4 substrate, with its dissolution into the slag. These observations are schematically represented in Figure 11 and are in agreement with the results described in our previous work,^[32] where the interaction between an identical synthetic $\text{PbO-CaO-SiO}_2\text{-Cu}_2\text{O-Al}_2\text{O}_3\text{-FeO-ZnO}$ slag and MgAl_2O_4 was examined in detail. It was proposed that the main reaction taking place at the studied MgAl_2O_4 –slag interface is as given in Reaction [1]:



In a simplified product between the slag and MgAl_2O_4 , the interaction or interfacial layer consists of $(\text{Mg,Fe})\text{Al}_2\text{O}_4$, as reported by Donald *et al.*^[31] The overall reaction was confirmed by thermodynamic calculations using FactSage, as described earlier.^[32] The good wetting between slag and spinel is consistent with previous research performed by Abdeyazan *et al.*,^[30] Tran *et al.*,^[38] and Donald *et al.*^[31]

From the screenshots, we observed that, with increasing time, the contact area between the liquid slag and the liquid copper droplet increases. Microstructural analysis

of the slag/copper droplet interface revealed a copper oxide–alumina layer at the interface, as indicated in Figure 9 and schematically represented in Figure 12.

Two possible explanations can be put forward for the presence of this layer. On the one hand, precipitation of Cu_2O at the slag–copper droplet interface is possible as a quenching effect. However, when considering the slag microstructure, no indications are found that quenching was not fast enough. Indeed, no precipitation of very small solid particles or very small dispersed copper droplets was detected, which are clear signs of too slow quenching. Therefore, it is less likely that this layer is a quenching effect. On the other hand, the layer can be assumed to originate from a reaction between the liquid slag and the copper droplet. An increased amount of copper is present in the slag next to the copper droplet, in the range of 5 to 9 wt pct, compared to the amount of copper present before the sessile drop experiment (1.3 wt pct). This points to a dissolution of copper into the slag. Additionally, the slag spreads spontaneously on the copper droplet. (Figure 2, 360 seconds at 1523 K (1250 °C)), which might be an additional indication of reactive wetting behavior between the Cu and slag.

Throughout the interaction between the slag and copper droplet, an emulsification process might have taken place. Chung^[39] described that during reactions between two fluids in reactive systems, several processes can occur such as a decrease in apparent interfacial energies, spontaneous spreading of droplets, spontaneous emulsification, and spontaneous surface creation. In an extensive study on the reactive wetting between steel alloys and slag, Chung^[39] and Rhamdhani^[40] observed an emulsification. Based on these observations, a mechanism was proposed including experiments demonstrating reactive wetting between steel alloys and slag. For the present experiment, no signs of an emulsification could be observed from the obtained micrographs. However, due to the dynamic nature of the observed phenomena, an emulsification cannot be excluded either.

B. Initialization Mechanism for New Sticking Copper Droplets in the Slag

Due to the very low weights of the used copper and slag, the copper–MgAl₂O₄, slag–MgAl₂O₄, and copper–slag interfacial tensions are determining and gravity effects are negligible for the behavior of both slag and copper on the substrate. Based on the behavior of the slag and copper droplets, it seems that the copper–spinel interaction is not stable in the presence of a slag. This is in contradiction with the presence of the small entrained sticking copper droplets in the slag droplet, and with the observations of the attached droplets in slags in our previous work.^[13,24] In this respect, we already demonstrated previously that an attached copper droplet is more stable from a thermodynamic point of view than a non-attached droplet, assuming that the surface of the droplet does not change after the attachment and if the following condition is valid:^[24]

$$\gamma_{\text{Sl-Cu}} + \gamma_{\text{Sp-Sl}} \geq \gamma_{\text{Sp-Cu}} \quad [2]$$

where $\gamma_{\text{Sl-Cu}}$ is the slag–copper interfacial tension, $\gamma_{\text{Sp-Sl}}$ is the spinel–slag interfacial tension, and $\gamma_{\text{Sp-Cu}}$ is the spinel–copper interfacial tension. Two explanations are suggested to interpret this dissimilarity in behavior between the performed sessile drop experiment and the phenomenon of sticking droplets.

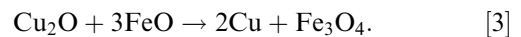
For one explanation, the surrounding gas of the copper droplet (*i.e.*, in the present experiments) contacting the slag in industry influenced the decisive interfacial tensions. The composition of the spinel substrate, the composition of the slag, and the dissolved oxygen level of the system can also influence the differences in interfacial tensions, as suggested in Eq. [2]. Furthermore, quantitative information on the interfacial tensions among phases is needed to properly assess the deciding factor for the mechanical entrainment of Cu droplets by spinel particles. At present, only limited data are available on copper–slag interfacial tensions for calcium ferrite slags,^[41] and to our knowledge, no data are available for $\gamma_{\text{Sp-Cu}}$ or $\gamma_{\text{Sp-Sl}}$.

For an alternative explanation, the origin of sticking droplets can also be found in a chemical mechanism, as elaborated in our previous work, where the formation of spinel solids around copper droplets was studied.^[24] Two possible pathways were proposed whereby the spinel solids form around the copper droplets or form simultaneously with the copper droplets, depending on the local composition of the system.^[24]

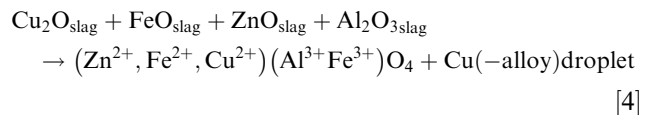
To explain the origin of the small entrained sticking droplets within the slag droplet in the present sessile drop experiment (zone III), a mechanism is proposed, which is schematically represented in Figure 13. As already mentioned above, copper dissolves from the copper droplet into the slag system. This was confirmed by higher copper levels in the slag around the copper droplet. Within the slag droplet, no metallic copper droplets were present in region (IV), directly next to the copper droplet, as shown in the LOM of Figure 3. This can be explained by two effects. Firstly, the absence of copper droplets can be linked to an Ostwald ripening effect occurring in the slag phase positioned directly next

to the big copper droplet. Secondly, it is also assumed that the slag next to the copper droplet locally has a higher copper solubility as compared to slag regions further away from the copper droplet (zone III). This gradient in copper solubility can possibly be linked to a gradient in oxygen level. Higher levels of oxygen result in higher amounts of dissolved copper, as experimentally observed by Somerville *et al.*^[42] and Nagamori *et al.*^[43] The oxygen level gradient within the slag droplet can be linked with an oxygen exchange between the copper droplet and the surrounding slag phase. This would cause higher oxygen levels in the slag region positioned directly around the copper droplet, and in that way would both explain the higher solubility of copper. In addition to the copper dissolution in the slag, copper diffusion away from the slag–droplet interface is expected to take place. Diffusional data for oxygen diffusion through both the slag^[44] and Cu droplet^[45,46] can be used to estimate the characteristic diffusion lengths. For oxygen in the metallic phase, this is 1.03 cm and for O in the slag phase, 0.16 cm. This vouches for the fact that even though the residual oxygen can react across the entire system—slag, liquid Cu, and MgAl₂O₄—it will mainly diffuse through the copper liquid phase.

It is assumed that those regions are characterized by lower copper solubility which will result in the precipitation of copper droplets. Thus, reactions with other oxides (*e.g.*, FeO) can occur, forming more stable oxides (*e.g.*, Fe₃O₄) and metallic copper. For example, during primary copper production, cuprous oxide reacts with ferrous oxide as follows^[6,20,23]:



Spinel-forming components present in the slag may also form spinel solids, according to the following overall reaction:



The presence of an increased level of ‘FeO’ in the spinel solids which are attached to copper droplets is in agreement with this assumption (Table V).

Within the proposed reaction mechanism, diffusion plays an important role. It is assumed that copper diffusion takes place at a significantly higher rate than oxygen diffusion. Consequently, a gradient in oxygen is present and influences the copper solubility in the slag droplet. Concerning the diffusion of both copper and oxygen through this slag, limited literature data are available on diffusion coefficients of these elements obtained under comparable experimental conditions. The limited data found in the Reference 47 for Cu and Reference 44 for O have overlapping values and were not obtained for comparable experimental conditions. In addition, it is also unclear what the p_{O₂}-influence on these diffusion coefficients is. However, the diffusion coefficients of these elements are known to be inversional to the radius of the ion through the slag.^[48] As

O²⁻ (0.140 nm) is known to have a bigger radius in comparison to the Cu²⁺ cations (0.096 nm), from which it can be expected that the diffusion coefficient will be smaller for oxygen.^[49] Additionally, slags are frequently used to seal of liquid metal from oxygen and prevent oxidation, because of the slow diffusion of oxygen through slag.^[50]

The reaction kinetics for the formation of spinel solids within the slag plays an essential role. Within different types of experimental publications, the fast formation of spinel solids has already been observed. Nightingale and Monaghan^[51] observed the formation of spinel crystals within seconds after the submersion of MgAl₂O₄ in a slag containing CaO, Al₂O₃, and SiO₂. Scheunis *et al.*^[52] investigated the interaction between magnesia chromite refractory and a spinel saturated PbO non-ferrous slag, for which the formation of a new spinel layer with a growth rate of 290.5 μm²/h was observed. Although this experiment was carried out on lab scale, it presents information relevant for industrial processes as it shows that sticking droplets can occur when all conditions are fulfilled to simultaneously form both spinel particles and copper droplets in the slag. Heterogeneities in an industrial slag phase can explain why these droplets will not appear everywhere.

The stability of the attached droplets originating from a chemical reaction is also expected to be subject to Eq. [2]. However, as long as the chemical reaction is not finished, a reactive wetting behavior is expected to take place between the spinel substrate and the copper droplet. Therefore, this could be an explanation why droplets and spinel particles remain attached for a certain amount of time, depending on the reaction time.

V. CONCLUSION

In this paper, the phenomenon of sticking copper alloy droplets to spinel solids in slags, hindering the sedimentation of the droplets, is studied. Focus is placed specifically on the copper–spinel, slag–spinel, and slag–copper interactions. An adapted sessile drop experiment was performed, in which both copper and slag were placed on the spinel substrate. Pure copper, a synthetic PbO–CaO–SiO₂–Cu₂O–Al₂O₃–FeO–ZnO slag, and a MgAl₂O₄ substrate were used to represent the copper alloy droplets, industrial slag, and spinel solids, respectively.

Within the sessile drop experiment, the interfacial tensions were the main driving force due to the very low weights of the slag and copper. The slag displayed a very good wetting behavior on the MgAl₂O₄ substrate, with the opposite being the case for the copper droplet. This leads to the slag positioning itself in between the copper droplet and the spinel substrate. In this way, no direct interaction between the copper and the MgAl₂O₄ substrate was possible. Subsequently, the different interfaces were studied. A (Mg,Zn,Fe)(Al,Fe)₂O₄ interaction layer was formed at the slag–MgAl₂O₄ interface. At the slag–copper droplet interface, a copper oxide layer was present and copper dissolution into the slag was also observed.

Small entrained copper droplets sticking to spinel solids were present within the slag droplet. A mechanism is proposed to explain the presence of those sticking droplets. It is suggested that the spinel solids and copper droplets form together due to a simultaneous reduction of copper oxides into metallic copper and the oxidation of slag oxides into more stable spinel structures. As spinel solids are characterized by very fast formation rates, new spinel solids can form directly next to the metallic copper droplets, leading to copper droplets, which are attached to spinel solids.

ELECTRONIC SUPPLEMENTARY MATERIAL

The online version of this article (doi:10.1007/s11663-016-0805-8) contains supplementary material, which is available to authorized users.

REFERENCES

1. R. Degel, H. Oterdoom, J. Kunze, A. Warczok and G. Riveros, in *Proc. Conf. Third international platinum conference 'Platinum in Transformation*, The Southern African Institute of Mining and Metallurgy, Sun City, South Africa, October 2008, pp. 197–202.
2. I.-K. Suh, Y. Waseda, and A. Yazawa: *High Temp. Mater. Process. (Lond.)*, 1988, vol. 8, pp. 65–88.
3. J.L. Liow, M. Juusela, N.B. Gray, and I.D. Sutalo: *Metall. Mater. Trans. B*, 2003, vol. 34B, pp. 821–82.
4. N. Cardona, L. Hernandez, E. Araneda and R. Parra, in *Proc. Conf. Copper 2010*, vol. 7, GMDB, Hamburg, Germany, June 2010, pp. 2637–54.
5. N. Cardona, P. Coursol, P.J. Mackey, and R. Parra: *Can. Metall. Q.*, 2011, vol. 50, pp. 318–29.
6. I. Imris, M. Sanchez, and G. Achurra, in *Proc. 7th Int. Conf. on molten slags, fluxes and salts*, The South African Institute of Mining and Metallurgy, Johannesburg, South Africa, January 2004, pp. 177–82.
7. R. Sridhar, J. Toguri, and S. Simeonov: *Metall. Mater. Trans. B*, 1997, vol. 28B, pp. 191–200.
8. R. Minto and W.G. Davenport: *Can. Min. Metall. Bull.*, 1972, vol. 65, pp. C36–42.
9. S.W. Ip and J.M. Toguri: *Metall. Trans. B*, 1992, vol. 23B, pp. 303–11.
10. H.C. Maru, D.T. Wasan, and R.C. Kintner: *Chem. Eng. Sci.*, 1971, vol. 26, pp. 1615–28.
11. L. Andrews: *Faculty of Engineering, Built Environment and Information Technology*, University of Pretoria, Pretoria, 2008, pp. 19–28.
12. A. Malfliet, S. Lotfian, L. Scheunis, V. Petkov, L. Pandelaers, P.T. Jones, and B. Blanpain: *J. Eur. Ceram. Soc.*, 2014, vol. 34, pp. 849–76.
13. E. De Wilde, I. Bellemans, M. Campforts, A. Khaliq, K. Vanmeensel, D. Seveno, M. Guo, M. Rhamdhani, G.A. Brooks, B. Blanpain, N. Moelans, and K. Verbeken: *Mater. Sci. Technol.*, 2015, vol. 31, pp. 1925–33.
14. D. Poggi, R. Minto, and W. Davenport: *J. Met.*, 1969, vol. 21, p. 40.
15. H. Kim, B. Ozturk, and R.J. Fruehan: *ISIJ Int.*, 1998, vol. 38, pp. 430–39.
16. J. Savolainen, T. Fabritius, and O. Mattila: *ISIJ Int.*, 2009, vol. 49, pp. 29–36.
17. P.F. Tan: *JOM*, 2011, vol. 63, pp. 51–57.
18. I. Bellemans, N. Moelans, and K. Verbeken: *Comput. Mater. Sci.*, 2015, vol. 108, pp. 348–57.

19. S. Pirker: *Steel Res. Int.*, 2010, vol. 81, pp. 623–29.
20. I. Imris, in *Metallurgical and Materials Processing: Principles and Technologies, Vol 1: Materials Processing Fundamentals and New Technologies*, F. Kongoli, K. Itagaki, C. Yamauchi and H. Y. Sohn, San diego, CA, 2003.
21. Y. Takeda, in *Metallurgical and Materials Processing: Principles and Technologies, Vol 1: Materials Processing Fundamentals and New Technologies*, F. Kongoli, K. Itagaki, C. Yamauchi and H. Y. Sohn, 2003, pp. 341–57.
22. K. Genevski and V. Stefanova: *Can. Metall. Q.*, 2008, vol. 47, pp. 51–58.
23. H. Jalkanen, J. Vehvilainen, and J. Poijarvi: *Scand. J. Metall.*, 2003, vol. 32, pp. 65–70.
24. E. De Wilde, I. Bellemans, L. Zheng, M. Campforts, M. Guo, B. Blanpain, N. Moelans, and K. Verbeken: *Mater. Sci. Technol.*, 2015, DOI:10.1080/02670836.2016.1151998.
25. O.B. Kozlova and S.A. Suvorov: *Refractories*, 1976, vol. 17, pp. 763–67.
26. N. Fukami, R. Wakamatsu, N. Shinozaki, and K. Wasai: *Mater. Trans.*, 2009, vol. 50, pp. 2552–56.
27. P. Sebo, B. Gallois, and C.H.P. Lupis: *Metall. Trans. B*, 1977, vol. 8B, pp. 691–93.
28. B. Gallois and C.H.P. Lupis: *Metall. Trans. B*, 1981, vol. 12B, pp. 679–89.
29. E. De Wilde, I. Bellemans, M. Campforts, M. Guo, K. Vanmeensel, B. Blanpain, N. Moelans, and K. Verbeken, in *European Metallurgical Conference*, Düsseldorf, 2015, pp. 3–18.
30. H. Abdeyazdan, N. Dogan, M. Rhamdhani, M. Chapman, and B. Monaghan: *Metall. Mater. Trans. B*, 2014, vol. 46B, pp. 208–19.
31. J.R. Donald, J.M. Toguri, and C. Doyle: *Metall. Mater. Trans. B*, 1998, vol. 29B, pp. 317–23.
32. E. De Wilde, I. Bellemans, M. Campforts, M. Guo, B. Blanpain, N. Moelans, and K. Verbeken, *Trans. Nonferrous Met. Soc. China*, in press.
33. Y. Takeda, S. Nakazawa, and A. Yazawa: *Can. Metall. Q.*, 1980, vol. 19, pp. 297–305.
34. Y. Takeda, S. Ishiwata, and A. Yazawa: *Trans. Jpn. I. Met.*, 1983, vol. 24, pp. 518–28.
35. E. De Wilde, I. Bellemans, S. Vervynckt, M. Campforts, K. Vanmeensel, N. Moelans, and K. Verbeken, in *European Metallurgical Conference*, Weimar, 2013, pp. 161–74.
36. N. Eustathopoulos, M.G. Nicholas, and B. Drevet: *Wettability at High Temperatures*, 1st ed., Elsevier, New York, 1999.
37. C. Nexhip, R. Davidson, and S. Sun, in *Proc. 7th Int. Conf. on Molten Slags Fluxes and Slags*, The South African Institute of Mining and Metallurgy, Johannesburg, South Africa, January 2004, pp. 271–76.
38. T. Tran, D. Xie, and Y.B. Cheng, in *VII International Conference on Molten Slags Fluxes and Salts*, The South African Institute of Mining and Metallurgy, 2004.
39. Y. Chung and A.W. Cramb: *Metall. Mater. Trans. B*, 2000, vol. 31, pp. 957–71.
40. M.A. Rhamdhani, K.S. Coley and G.A. Brooks, in *43th Annual Conference of Metallurgists of CIM*, G. Irons and S. Sun, eds., Hamilton, Ontario, Canada, 2004, pp. 203–17.
41. T. Sakai, S.W. Ip, and J.M. Toguri: *Metall. Mater. Trans. B*, 1997, vol. 28B, pp. 401–07.
42. M. Somerville, S. Sun, and S. Jahanshahi: *Metall. Mater. Trans. B*, 2014, vol. 45B, pp. 2072–79.
43. M. Nagamori, P.J. Mackey, and P. Tarasoff: *Metall. Mater. Trans. B*, 1975, vol. 6B, pp. 295–301.
44. M. Sasabe and K.S. Goto: *Metall. Trans*, 1974, vol. 5, pp. 2225–2233.
45. K.E. Oberg, L.M. Friedman, W.M. Boorstei, and R.A. Rapp: *Metall. Trans*, 1973, vol. 4, pp. 75–82.
46. S. Otsuka and Z. Kozuka: *Metall. Trans. B*, 1976, vol. 7B, pp. 147–49.
47. F. Ajersch and J.M. Toguri: *Can. Metall. Q.*, 1970, vol. 9, p. 507.
48. Y. Oishi, R. Terai, H. Ueda, A.R. Cooper, and A.H. Heuer, in *Mass Transport Phenomena in Ceramics*, Springer US, New York, 1975, pp. 297–310.
49. W.D. Callister and D.G. Rethwish: *Materials science and engineering*. 8th ed. (2010).
50. V.V. Belousov: *Metall. Mater. Trans. A*, 2014, vol. 45A, pp. 4257–67.
51. S.A. Nightingale and B.J. Monaghan: *Metall. Mater. Trans. B*, 2008, vol. 39B, pp. 643–48.
52. L. Scheunis, M. Campforts, P.T. Jones, B. Blanpain, and A. Malfliet: *J. Eur. Ceram. Soc.*, 2015, vol. 35, pp. 347–55.